Coherent Compounding in Doppler Imaging

Ingvild K. Ekroll, Marco M. Voormolen, Oyvind K-V. Standal, Jochen M. Rau, and Lasse Lovstakken

***Abstract*—Coherent compounding can provide high frame rates and wide regions of interest for imaging of blood flow. However, motion will cause out-of-phase summation, potentially causing image degradation. In this work the impact of blood motion on SNR and the accuracy of Doppler velocity estimates are investigated. A simplified model for the compounded Doppler signal is proposed. The model is used to show that coherent compounding acts as a low-pass filter on the coherent compounding Doppler signal, resulting in negatively biased velocity estimates. Simulations and flow phantom experiments are used to quantify the bias and Doppler SNR for different velocities and beam-to-flow (BTF) angles. It is shown that the bias in the mean velocity increases with increasing beam-to-flow angle and/or blood velocity, whereas the SNR decreases; losses up to 4 dB were observed in the investigated scenarios. Further, a 2-D motion correction scheme is proposed based on multi-angle vector Doppler velocity estimates. For a velocity of 1.1 v_{Nyq} and a BTF angle of 75°, the bias was reduced from 30% to less than 4% in simulations. The motion correction scheme was also applied to flow phantom and *in vivo* recordings, in both cases resulting in a substantially reduced mean velocity bias and an SNR less dependent on blood velocity and direction.**

I. Introduction

The introduction of plane wave imaging, in which unfocused, full field-of-view transmit pulses are emitted and many or all image lines are beamformed in parallel on receive, has revealed significant potential for improving ultrasound color flow imaging (CFI). The approach enables higher frame rates and wide regions of interest; furthermore, it allows the use of higher temporal ensembles for improved clutter filtering and a higher measurable velocity scale [1]–[3]. The use of unfocused pulses, however, also introduces potential challenges. First, because of the lack of focusing, pressure deep in the tissue is substantially reduced compared with conventional imaging. This leads to the question of whether the achievable penetration is sufficient for all patients and clinical applications. Second, increased side lobe levels substantially reduce the contrast resolution in the image. In particular, this will potentially impair imaging of small vessels.

Coherent plane wave compounding has been proposed to overcome these challenges. The received images from several transmitted plane waves emitted from different angles are summed coherently (i.e., in phase) [4]. In this way, signal-to-noise levels are improved, transmit side lobe levels are decreased, and dynamic transmit focusing is achieved to significantly improve the overall image quality outside the conventional focal region [5]. For Doppler imaging, the coherent compounding concept was first described based on a synthetic transmit aperture (STA) approach. In this approach, spherical waves are emitted from single elements or smaller parts of the transducer aperture and utilized to form low-resolution images. These images are then combined coherently to produce a higher resolution image [6]. Such an approach can be utilized to achieve both high-frame-rate CFI and vector-Doppler imaging [7]. More recently, coherent compounding Doppler (CCD) imaging based on plane-wave imaging has been shown to provide high SNR and image quality when imaging small vessels, as well as retrospective PW-Doppler spectra which can be calculated from arbitrary regions in the 2-D image [2], [8].

Both approaches rely on the coherent summation of the received signal from several emissions to achieve coherent SNR gain and a proper reconstruction of a high-resolution point spread function (PSF). It is assumed that there is negligible motion in the time spanned by the summed emission sequence. Axial motion during the sequence can lead to out-of-phase summation resulting in spatial shifts of the point spread function and a loss in SNR gain [9]–[12]. Pure lateral motion is, on the other hand, expected to mostly smear the PSF, because of the lateral low-pass property of the imaging system. Because the stationarity assumption is inherently incorrect when imaging moving tissue or blood flow, some degradation of image quality is expected. The effects of tissue motion on B-mode image quality have been studied previously, and methods for axial and lateral correction of tissue motion have been shown to improve the image quality and SNR both in STA and coherent plane wave compounding [10], [12].

In this work we investigate the influence of blood motion in coherent compounding Doppler imaging. In particular, the influence of scatterer motion on SNR and mean frequency estimator accuracy is assessed. The acquisition concept is briefly revisited and a simplified signal model for the CCD signal is introduced. Further, a technique to compensate for the 2-D motion is proposed, utilizing vector-Doppler blood velocity estimates derived from the same group of tilted plane wave emissions. Using this method, we investigate the influence of both 1-D and 2-D motion compensation in CCD imaging. Simulations are used to evaluate the effects of motion for simplified scenarios, whereas a flow phantom setup is used to investigate the impact of motion and feasibility of motion correction in further detail. Finally, carotid artery flow

Manuscript received January 27, 2015; accepted June 23, 2015.

The authors are with the Department of Circulation and Medical Imaging, Norwegian University of Science and Technology, 7491 Trondheim, Norway (e-mail: ingvild.k.ekroll@ntnu.no).

I. K. Ekroll is also with St. Olav's University Hospital, 7006 Trondheim, Norway.

DOI http://dx.doi.org/10.1109/TUFFC.2015.007010

recordings from a healthy volunteer are used to demonstrate the potential impact and feasibility of the correction technique *in vivo*.

II. The Coherent Compounding Doppler Signal

A coherent plane wave compounding sequence consists of N successive emissions of unfocused transmit pulses with varying steering angles θ_n, at a firing pulse repetition frequency ($\mathrm{PRF}_{\max}$). A Doppler acquisition is obtained by repeating the compounding sequence at regular intervals, yielding a Doppler pulse repetition frequency (PRF), and the CCD signal is therefore defined in two slow-time domains. The compound domain in which the coherent summation is performed has a sampling frequency of $\mathrm{PRF}_{\max}$ and is indexed using n. The Doppler domain in which the velocity estimation is performed has a sampling frequency of PRF and is indexed by m.

The Doppler PRF determines the Nyquist velocity v_{Nyq} and is dependent on the application. Because the maximum firing rate is dictated by the imaging depth, the maximal number of transmit events in the compounding sequence is restricted to $N = \mathrm{PRF}_{\max}/\mathrm{PRF}$, where it is necessary that $N \geq 2$ to do coherent compounding. For general vascular and slow-flow imaging this requirement is typically fulfilled ($N \approx 2$ to 16), but this is not the case for cardiac imaging because of the imaging depth and high blood velocities.

To obtain an expression for the CCD signal, it is convenient to consider in-phase and quadrature (IQ) signals which are continuous in slow-time. In the following, these ideal signals from an arbitrary image point will be denoted by $s_{\theta_n}(t,\mathbf{r})$, where $\mathbf{r}$ is spatial position and θ_n is the steering angle of transmit event n. The CCD signal is found by adding $s_{\theta_n}(t,\mathbf{r})$ coherently for each group of N emissions, with an appropriate delay of $\Delta t = 1/\mathrm{PRF}_{\max}$ to account for the time between successive emissions:

$$c(t,\mathbf{r}) = \sum_{n=0}^{N-1} w_n s_{\theta_n}(t + n\Delta t, \mathbf{r}). \tag{1}$$

Here, w_n indicates amplitude weighting of signals originating from different transmit events. The CCD signal in the Doppler domain is obtained by sampling $c(t,\mathbf{r})$ at $t = mN\Delta t$.

The frequency-domain representation of the CCD signal is found by applying the temporal Fourier transform to (1), resulting in

$$C(\omega,\mathbf{r}) = \sum_{n=0}^{N-1} w_n e^{i\omega n\Delta t} S_{\theta_n}(\omega,\mathbf{r}). \tag{2}$$

From (2), it is observed that the time-shift between successive transmit events results in a complex weighting of the N spectra $S_{\theta_n}(\omega,\mathbf{r})$, where the phase shift is determined by the firing rate of the compound sequence, $\Delta t = 1/\mathrm{PRF}_{\max}$.

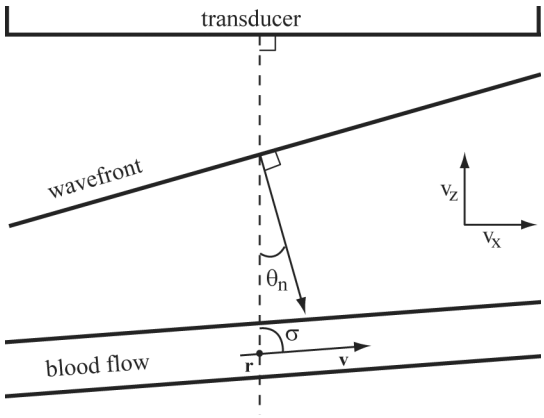

Fig. 1. A schematic illustration of the wavefront from a plane wave approaching a blood vessel. In coherent compounding, a set of N successive plane waves separated in time by $\Delta t = 1/\mathrm{PRF}_{\max}$ are transmitted. The transmit angles θ_n are symmetrically distributed around 0. For a given image point $\mathbf{r}$, the angle between the transducer normal and the flow direction is σ, hereafter referred to as the reference beam-to-flow angle.

A. Coherent Compounding as a Low-Pass Filtering Effect

Assuming that the N different $S_{\theta_n}(\omega,\mathbf{r})$ are identical except for a scaling of the frequency axis to account for the different beam-to-flow angles, (2) yields:

$$C(\omega) = \sum_{n=0}^{N-1} w_n e^{i\omega n\Delta t} S_{\theta_n}\left(\frac{\omega}{\cos\sigma}\cdot\cos(\sigma+\theta_n)\right). \tag{3}$$

Because the effect of compounding is independent of spatial coordinates, $\mathbf{r}$ has been left out for simplicity. As indicated in Fig. 1, it is assumed that the transmit angles θ_n are spaced symmetrically around a center angle of 0°, in which case the angle σ between the transducer normal and the flow direction acts as the reference beam-to-flow angle. If the transmit angles span a small sector, $S_{\theta_n}(\omega) \approx S_\sigma(\omega)$, and (3) can be reduced to

$$C(\omega) = \sum_{n=0}^{N-1} w_n e^{i\omega n\Delta t} S_\sigma(\omega) \equiv H_N(\omega) S_\sigma(\omega). \tag{4}$$

Assuming a standard weighting window with real and positive coefficients w_n, (4) shows that coherent compounding in the most straightforward interpretation acts as a simple FIR low-pass filter with coefficients and cut-off frequency determined by the number of transmissions, the weighting w_n and $\mathrm{PRF}_{\max}$.

B. Influence of Blood Motion in CCD Imaging

In Doppler imaging, the Nyquist velocity corresponds to a spatial shift in scatterer position of $v_{\mathrm{Nyq}}/\mathrm{PRF} = \lambda/2$ in the effective transmit/receive direction. Blood motion in the transverse direction will increase the bandwidth of the Doppler signal by decreasing the transit time of the scatterers for typical imaging setups. Two effects should be noted when motion is present in CCD imaging. First, as a consequence of the low-pass filter effect, the com-

pounded slow-time signal sampled at the Doppler PRF may yield negatively biased velocity spectra and/or mean frequency (autocorrelation) estimates. As seen from (4), the magnitude of the bias is directly related to the velocity in the effective transmit/receive direction. However, the effect of transversal motion enters implicitly through a broadening of the individual frequency spectra. As $H_N(\omega)$ shifts the distribution of spectral power toward zero by attenuating higher frequencies, broadband signals will be more influenced by the filter and therefore yield a larger negative bias.

Second, blood motion will also limit the SNR gain expected from coherent compounding because of out-of-phase summation. As previously described for STA imaging in [11], the degradation in SNR is expected to reach its maximum for axial motion corresponding to complete destructive interference between two transmissions, namely at $v/\mathrm{PRF}_{\max} = \lambda/4$. Such spatial shifts correspond to velocities far beyond the Nyquist limit in typical imaging setups for coherent compounding ($N = 2$ to $16 \rightarrow v/\mathrm{PRF} = \lambda/2$ to 4λ). However, a decreased SNR can also be expected for velocities relevant for imaging of blood flow, with a decrease of approximately 2 dB reported for velocities close to the Nyquist limit [10], [11]. Because the SNR in blood flow imaging can be very low, a 2 dB loss in SNR may significantly reduce image quality.

II. Material and Methods

A. Multi-Angle Vector Doppler

The coherent compounding sequence may be used to generate a color flow image from each individual transmit angle. This information can be combined to yield vector Doppler images as well. The vector velocity $\mathbf{v} = [v_x, v_z]$ is estimated from the N Doppler frequency estimates in every point of the image using the relation

$$\hat{\mathbf{f}} = k\mathbf{A}\mathbf{v}, \tag{5}$$

where $\hat{\mathbf{f}} = [\hat{f}_0 \ldots \hat{f}_{N-1}]^{\mathrm{T}}$ is a vector containing the Doppler frequency estimates from the N transmit angles and k is a factor converting frequency to velocity. Using a crossed-beam vector-Doppler scheme with a common receive direction normal to the transducer surface, $\mathbf{A}$ is an $N \times 2$ matrix with rows [13], [14]

$$\mathbf{a}_n = [-\sin\theta_n, 1 + \cos\theta_n], \tag{6}$$

in which θ_n is the steering angle of transmission n.

B. Motion Correction

Based on the 2-D blood velocity estimates, a motion correction technique is proposed to compensate for the *in-frame* motion which degrades the coherence of the summed transmissions. The time of transmission of the center angle is used as a reference. For a certain region of interest, 2-D interpolation of the individual plane wave signals using the calculated displacement is performed, providing a motion-corrected CCD signal

$$\tilde{\underline{c}}(m, \mathbf{r}) = \sum_{n=0}^{N-1} \underline{s}_{\theta_n}(mN + n, \tilde{\mathbf{r}}_n) e^{-i2\pi v_z(m,\mathbf{r})\tau_n/c_0}, \tag{7}$$

where $\tilde{\underline{c}}(m) = \tilde{c}(mN\Delta t)$, $\underline{s}_{\theta_n}(l) = s_{\theta_n}(l\Delta t)$, and

$$\tilde{\mathbf{r}}_n = \mathbf{r} + \tau_n \begin{pmatrix} -1 & 0 \\ 0 & 1 \end{pmatrix} \mathbf{v}, \quad \tau_n = \frac{n - (N-1)/2}{\mathrm{PRF}_{\max}}.$$

The exponential term in (7) is a demodulation phase correction factor required when motion correction is done on IQ data. The speed of sound is denoted by c_0.

C. Simulations

To quantify the impact of *in-frame* motion on Doppler velocity estimation and SNR, simulations were performed using Field II [15]. Because imaging of small blood vessels is the typical coherent compounding application, a simulation setup reflecting this scenario was chosen (see Table I). Single-plane-wave ($\theta = 0°$) point scatterer simulations were conducted to provide Doppler frequency spectra utilized for the FIR filtering interpretation of coherent compounding in Doppler imaging, whereas plug flow simulations (10 scatterers per resolution cell) were used to quantify mean velocity bias and Doppler SNR. The number of Doppler samples acquired is referred to as the ensemble length in all tables. Thermal (white) noise was added to the simulated channel data to yield a SNR of approximately 10 dB before beamforming and compounding. Mean velocity estimates were calculated using the autocorrelation technique [16], using an averaging area of approximately 3.5 × 5 mm, located well within the overlap region of all transmit angles.

Beam-to-flow angles of 0°, 45°, 70°, and 75° were simulated in the case of plug flow, with scatterer velocities ranging from 0.2 to 1.1 times the Nyquist limit in the z-direction. See Table I for further specifications. Weighting of the signal amplitudes originating from different transmit events was implemented by removing the first and last

TABLE I. Simulation Parameters.

Parameter	Value
Probe type	128-element linear array
Active transmit elements	128
Pitch [μm]	100
Transmit frequency [MHz]	13.3
Pulse periods	2.5
$\mathrm{PRF}_{\max}$ [kHz]	15
Doppler PRF [kHz]	1
Number of transmit angles	15
Transmit angles, θ_n [°]	$-8 \rightarrow 8$
Ensemble length	50
Receive angle [°]	0
Receive f-number	1.4
Clutter filter	No

TABLE II. PARAMETERS USED IN FLOW PHANTOM EXPERIMENTS.

Parameter	Plane wave	Conventional
Probe type	L9–4/38	L9–4/38
Active transmit elements	128	46
Pitch [μm]	304	304
Transmit frequency [MHz]	5	5
Pulse periods	2.5	2.5
PRF_{max}[kHz]	15	15
Doppler PRF [kHz]	1	1
Number of transmit angles/beams	15	60
Transmit angles, θ_n [°]	$-8 \rightarrow 8$	0
Ensemble length	100	45
Receive angle [°]	0	0
Receive f-number	1.4	1.4
Clutter filter (polynomial order)	3	1

element of a Tukey window of length $N + 2$ with cosine tapering ratio $\rho = 0.5$. This value of ρ was chosen to act as a compromise between rectangular ($\rho = 0$) and Hann windowing ($\rho = 1$).

Both 1-D (z) and 2-D (x and z) velocity estimates were used when quantifying the effect of motion correction. Further, both the ground truth velocity (GT) and the corresponding vector Doppler (VD) estimate of $\mathbf{v}$ were used (separately).

D. Flow Phantom Experiments

To investigate the feasibility and effect of motion correction, flow phantom studies were performed. A custom made flow phantom was constructed for this purpose, similar to the one described in Rickey *et al.* [17]. For the phantom, 1.5% (by weight) agar was used (Agrose A0169, Sigma-Aldrich, Madrid, Spain) as the tissue-mimicking material (TMM) with 0.1% 6-μm silicon carbide particles (Carborex F800, Washington Mills, Orkanger, Norway) to provide some background scattering. Four wall-less vessels with diameters of 0.7 mm were molded in the TMM with beam-to-flow angles of 50°, 60°, 70°, and 75°. For the blood-mimicking fluid, the recipe of Ramnarine *et al.* [18] was followed. Approximately 2% (by weight) of 5-μm Orgasol particles (Atofina, Oakville, Canada) was dissolved in water after wetting it in approximately 0.9% surfactant (Sun Rinse Aid, Unilever, Rotterdam, The Netherlands). A syringe pump (Alaris CC, Cardinal Health, Rolle, Switzerland) was used to provide accurate and steady flow through the phantom.

Measurements were performed with the Ultrasonix L9-4/38 transducer connected to a SonixMDP scanner (Analogic Corp., Richmond, BC, Canada), utilizing a SonixDAQ (Analogic Corp.) to acquire pre-beamformed channel data. Flow velocities were chosen to approximate those used in simulations, ranging from 0.2 to 1.1 times the Nyquist limit in the z-direction. Plane-wave and conventional focused recordings were interleaved for comparison for each flow velocity and each BTF angle. Flow phantom parameters, scanner settings, and post-processing parameters for both recording methods are listed in Table II.

TABLE III. *IN VIVO* IMAGING AND PROCESSING PARAMETERS.

Parameter	Value
Probe type	L9–4/38
Active transmit elements	128
Pitch [μm]	304
Transmit frequency [MHz]	5
Pulse periods	2.5
PRF_{max} [kHz]	15
Doppler PRF [kHz]	3
Number of transmit angles	5
Transmit angles, θ_n [°]	$-10 \rightarrow 10$
Ensemble length	Continuous
Receive angle [°]	0
Receive f-number	1.4
Clutter filter	92 tap FIR
Clutter filter cutoff [cm/s]	1.7
PW window size	128
Autocorr window size	32

E. In Vivo *Experiments*

A CCD imaging sequence with 5 transmit angles was used to record data from the common carotid artery of a healthy volunteer. Imaging parameters are listed in Table III. Using a PRF_{max} of 15 kHz resulted in a Nyquist velocity approximately equal to the peak (mean) velocity in the z-direction. PW Doppler spectra and autocorrelation velocity estimates were compared using single-plane-wave data ($\theta = 0°$) and compounded data from the same acquisition. A sample volume in the middle of the vessel was extracted from the data. Spectral estimation was performed using the Welch technique with a (sliding) window of 128 samples, whereas a (sliding) window of 32 samples was used to provide autocorrelation estimates. Vector velocity estimates based on the approach described in Section II-A were used for motion correction, as described in Section II-B.

III. RESULTS

A. Signal Model Predictions

Fig. 2(a) shows (the frequency response of) $H_N(\omega)$ for values of N between 2 and 20 ($w_n = 1$ for all n). The frequency axis is normalized by the Nyquist frequency, f_{Nyq}. The figure shows that the number of transmissions N does not have a large impact on the frequency response of the filter; frequencies close to and beyond the Nyquist limit will be attenuated similarly independent of the number of compound angles.

Fig. 2(b) shows the frequency response of $H_N(\omega)$ for values of N between 2 and 20, using a Tukey window with a cosine tapering ratio of 0.5 as weighting function. Transmit apodization is commonly used to decrease the side lobe level of the point spread function, but as shown here, weighting of the signal amplitudes from different transmit events also results in a broadening of the effective low-pass filter. As a consequence, such weighting has the potential to reduce the negative bias in Doppler velocity estimates caused by the coherent compounding process.

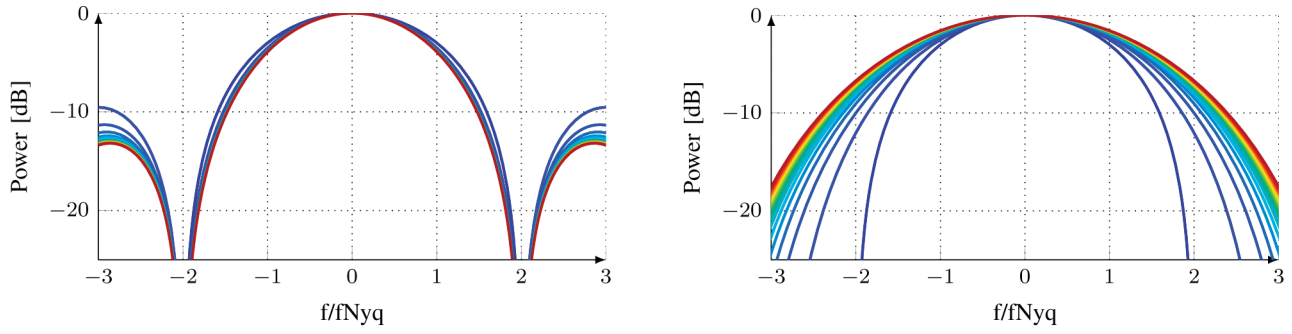

Fig. 2. Power of the effective low-pass filter $H_N(\omega)$ for values of N between 2 (dark blue) and 20 (dark red). With an axis normalized with the Nyquist frequency, f_{Nyq}, it can be observed that the frequency response (phase not shown) changes little with N when rectangular weighting is used. Applying a (nonrectangular) window results a spectral width of $H_N(\omega)$ that increases with N.

Figs. 3(a) and 3(b) show how coherent compounding acts in the compound and Doppler frequency domain respectively. The example illustrates a situation with a large beam-to-flow angle (75°) and a mean velocity of $1 \cdot v_{\text{Nyq}}$ in the reference direction (center angle). Higher frequencies are attenuated more, resulting in asymmetric Doppler spectra and a shift in the distribution of spectral power toward zero. This also results in negatively biased mean frequency estimates.

Fig. 4(a) shows the expected mean velocity bias using the low-pass filter interpretation for situations of varying blood velocity and beam-to-flow angle; a large angle in this scenario giving a shorter transit time and broadening of the Doppler frequency spectrum. For BTF angles between 0° and 45° the bias is smaller than 3% in all cases. For beam-to-flow angles larger than 45°, the negative bias has a substantial increase in magnitude with increasing velocity and BTF angle, reaching a maximum of more than 30% in the worst case (75° BTF angle and velocity 1.1 times the Nyquist limit).

B. Plug Flow Simulations

1) Mean Velocity Bias: Fig. 4(b) shows the bias in mean velocity estimates as a function of normalized velocity using rectangular weighting ($w_n = 1$ for all n). As predicted by the signal model and the low-pass filter interpretation of CCD imaging, the magnitude of the bias increases both with increasing velocity and with increasing BTF angle. At velocities of $0.2 \cdot v_{\text{Nyq}}$, the bias magnitude was below 4% for all beam-to-flow angles. At 0.4 and $0.8 \cdot v_{\text{Nyq}}$, negative biases of 1% to 5% and 2% to 18% were observed, whereas velocities of $1.1 \cdot v_{\text{Nyq}}$ resulted in a negative bias of 3% to 32% for beam-to-flow angles of 0° to 75°, respectively.

Fig. 5(a) demonstrates that non-rectangular weighting may be used to obtain some reduction of the bias in Doppler velocity estimates. However, using a Tukey window ($\rho = 0.5$) there is still a bias of approximately −25% in the worst-case scenario.

Figs. 6(a) and 6(b) show that although 1-D motion correction results in a reduction of the bias, 2-D correction is needed to get a substantial improvement in the accuracy of CCD velocity estimates, especially for flows with a large lateral velocity component. Whereas in the worst case a bias of −16% was still present after 1-D motion correction, 2-D motion correction could reduce the bias to less than −4% for all investigated scenarios. Fig. 6(b) shows that the difference between the use of the known flow velocity (GT) and the estimated velocity components from vector

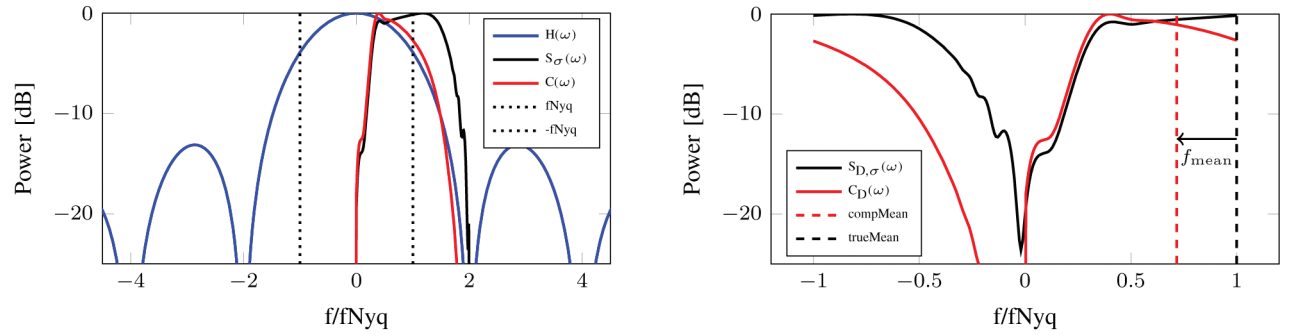

Fig. 3. (a) Power of the effective low-pass filter $H_N(\omega)$, the reference frequency spectrum $S_\sigma(\omega)$, and the compound frequency spectrum $C(\omega)$ in the compound (PRF_{max}) domain. The black dotted lines indicate the Nyquist limits in the Doppler (PRF) domain. (b) Power of the reference frequency spectrum $S_\sigma(\omega)$ (black) and the compound frequency spectrum $C(\omega)$ (red) in the Doppler domain. The black arrow indicates the shift in estimated mean frequency.

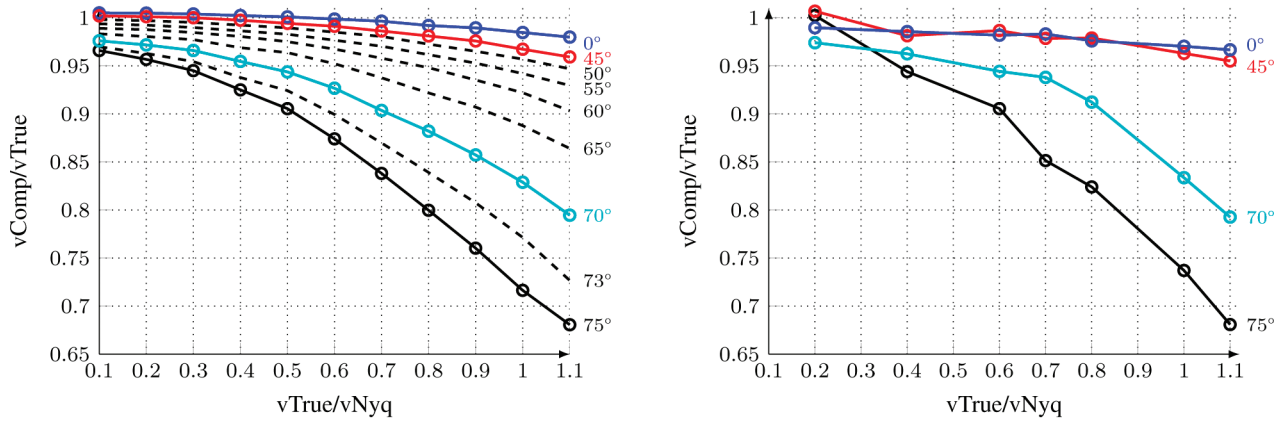

Fig. 4. (a) The predicted bias (vEst/vTrue) as a function of normalized velocity using the approximation in (4). Beam-to-flow angles 0° (blue), 45° (red), 70° (cyan), and 75° (black) are emphasized with color and markers. (b) Estimated bias (vComp/vTrue) as a function of normalized velocity for the plug flow simulation scenarios with beam-to-flow angles 0° (blue), 45° (red), 70° (cyan), and 75° (black).

Doppler (VD) was negligible (in the high-velocity cases, a simple unwrapping scheme was utilized to avoid degradation of the VD estimates due to aliasing).

2) Signal-to-Noise Ratio: Fig. 5(b) shows the SNR in simulated CCD power Doppler images using rectangular windowing of the echo amplitudes from different transmit angles. When increasing the velocity from $0.2 \cdot v_{\mathrm{Nyq}}$ to $1.1 \cdot v_{\mathrm{Nyq}}$, the SNR was reduced by approximately 4 dB for all beam-to-flow angles. Figs. 5(c) and 7 show that whereas the use of transmit event weighting resulted in a slightly reduced SNR at low velocities, the use of motion correction resulted in a gain in SNR at higher velocities, resulting in a signal-to-noise ratio which was less dependent on velocity. It was also observed that 1-D and 2-D motion correction resulted in similar SNR gain.

C. Flow Phantom Experiments

1) Mean Velocity Bias: The top panel in Fig. 8 shows mean velocity estimates from the flow phantom experiment. As in simulations, a large beam-to-flow angle and/or high velocity magnitude resulted in a substantial negative mean velocity bias when using coherent compounding Doppler imaging, which was not present when using conventional (focused) Doppler imaging. In the measured velocity interval, the bias magnitude increased from 7% to 30% and 2% to 20% for BTF angles 74° and 60°, respectively, but was substantially reduced using the 2-D motion compensation scheme. Exceptions are found at $v_{\mathrm{Pump}}/v_{\mathrm{Nyq}} \approx 0.5$ and ≈ 0.7 in the 60° case. This is probably because of the presence of high-velocity air bubbles resulting in erroneous velocity estimates and further causing the correction scheme to fail.

2) Signal-to-Noise Ratio: The bottom panel in Fig. 8 shows estimated SNR from CCD power Doppler images from the same experiment. In the case of a 74° beam-to-flow angle, the CCD SNR clearly decreased with increasing velocity magnitude; an increase in the velocity from $0.1 \cdot v_{\mathrm{Nyq}}$ to $0.7 \cdot v_{\mathrm{Nyq}}$ resulted in a reduction of the SNR by ≈ 2 dB. As in simulations, the SNR could be restored after use of motion correction based on the proposed multi-angle vector Doppler scheme. Again, the presence of bubbles in the 60° case at $v_{\mathrm{Pump}}/v_{\mathrm{Nyq}} \approx 0.5$ and ≈ 0.7 is believed to cause a less clear trend, as the bubbles in these cases introduced an artificially high SNR compared with the measurements without bubbles.

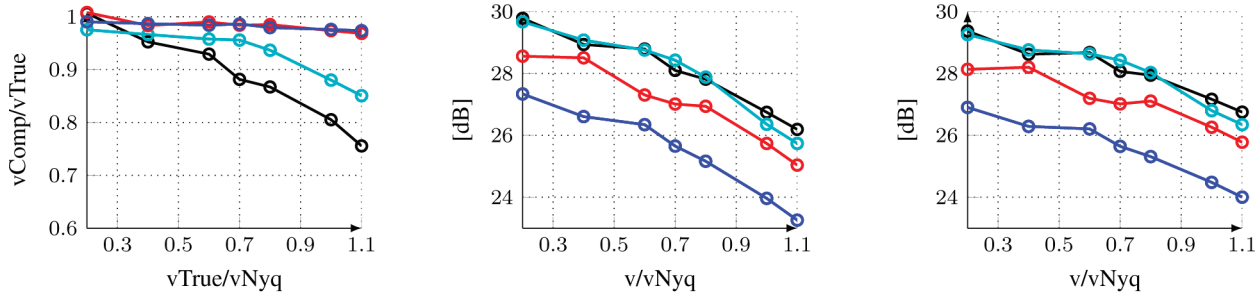

Fig. 5. Plug flow simulation results showing (a) mean velocity bias with Tukey weighting, (b) SNR with rectangular weighting, and (c) SNR with Tukey weighting. Beam-to-flow angles are 0° (blue), 45° (red), 70° (cyan), and 75° (black).

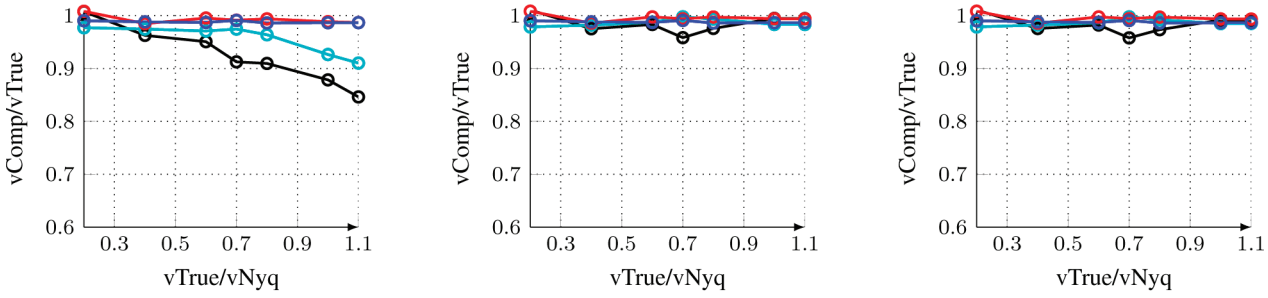

Fig. 6. Plug flow simulation results showing mean velocity bias after (a) 1-D motion correction (GT), (b) 2-D motion correction (GT), and (c) 2-D motion correction (VD). Beam-to-flow angles are 0° (blue), 45° (red), 70° (cyan), and 75° (black). 2-D motion correction resulted in a substantial decrease in mean velocity bias compared with 1-D motion correction.

D. Coherent Compounding In Vivo

Fig. 9 shows PW Doppler spectra and mean velocity estimates using single plane wave (left) and coherent compounding (right) data, respectively. The single-plane-wave Doppler spectrum acts as the reference, with a transmit angle equal to the transducer normal. In the single-plane-wave case, the mean velocity is approximately equal to the Nyquist velocity in systole. As expected, there was little difference between single-plane-wave imaging and coherent compounding at low velocities (in diastole). However, the high blood velocity in systole gives rise to a negative bias in the case of coherent compounding, reaching a maximum of −16% in peak systole. Because the estimated flow direction in systole was 70° to 75°, this corresponds reasonably well to the expected bias predicted from the model and plug flow simulations. As seen from the PW Doppler spectra, a trace of the envelope (peak velocities) would also give a large negative bias compared with single-plane-wave imaging, because the spectral power in systole is reduced by approximately 6 dB. This is also illustrated in Fig. 11, showing the averaged spectral power in mid-systole as a function of axial velocity.

The left panel of Fig. 10 shows the CCD PW Doppler spectrum when motion correction is applied. It can be observed that the spectral power at high velocities is regained and that the mean velocity estimate again reaches the Nyquist limit in peak systole. The boxplot in the right panel gives an impression of the bias present in systolic and diastolic mean velocity estimates when using CCD imaging *in vivo*—before (blue boxes) and after (red boxes) motion correction. Systolic velocities are defined as all mean velocity estimates in 40 ms around peak systole. A temporal window of 0.5 s was used for the diastolic mean velocities. The boxes represent the mean velocity values by the median and the 25th and 75th percentiles, whereas the whiskers account for the remaining mean velocity measurements. Because the velocities are higher during systole, the bias magnitude in that temporal segment is significantly larger than during diastole. Some residual bias is still present in the mean velocity estimates also after motion correction is performed, approximately −4% during systole.

IV. Discussion

In this work, the effect of 2-D motion on coherent compounding Doppler imaging has been investigated. More specifically, the impact of blood motion on SNR and spectral and mean velocity estimates has been quantified for different beam-to-flow angles and blood velocities. It was found that the use of compounding leads to a bias toward zero in Doppler velocity estimates. The bias magnitude increases with increasing velocity or beam-to-flow angle. Using a simple model for the CCD signal, this effect could in the most straightforward case be shown to equal the effect of an FIR low-pass filter.

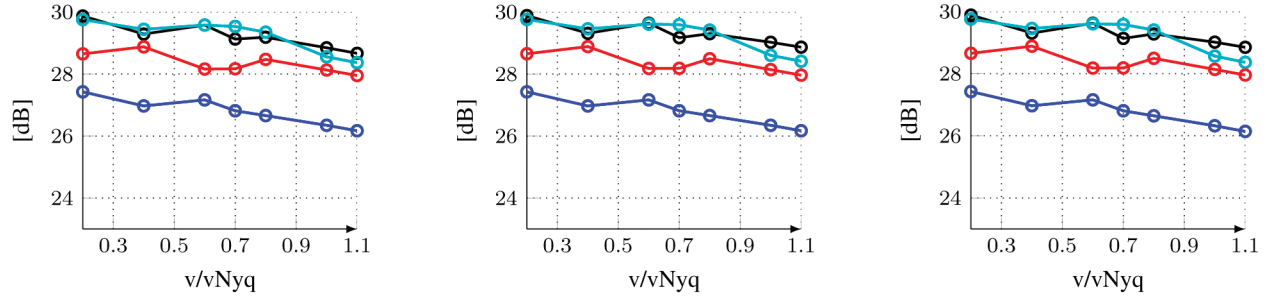

Fig. 7. Plug flow simulation results showing SNR after (a) 1-D motion correction (GT), (b) 2-D motion correction (GT), and (c) 2-D motion correction (VD). Beam-to-flow angles are 0° (blue), 45° (red), 70° (cyan), and 75° (black). 1-D and 2-D motion correction resulted in similar SNR gain.

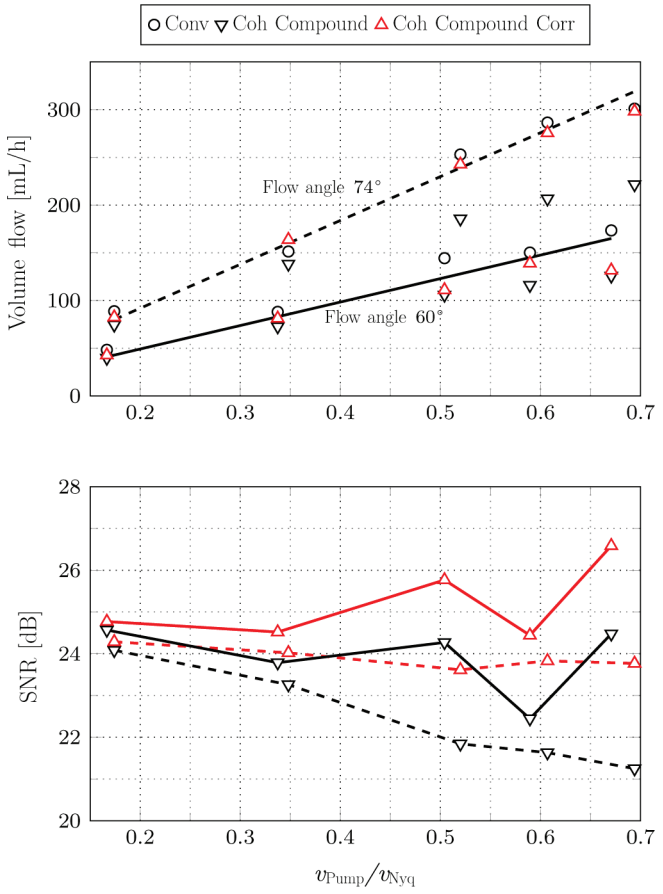

Fig. 8. (top): Estimates of volume flow based on mean velocity estimates. Straight lines indicate expected output from the syringe pump in the case of a 74° (dashed) and 60° (solid) beam-to-flow angle. (bottom): SNR before and after motion correction for the two beam-to-flow angles. In both panels, downward pointing triangles mark coherent compounding and upward pointing triangles mark coherent compounding with motion compensation. Circles mark conventional imaging.

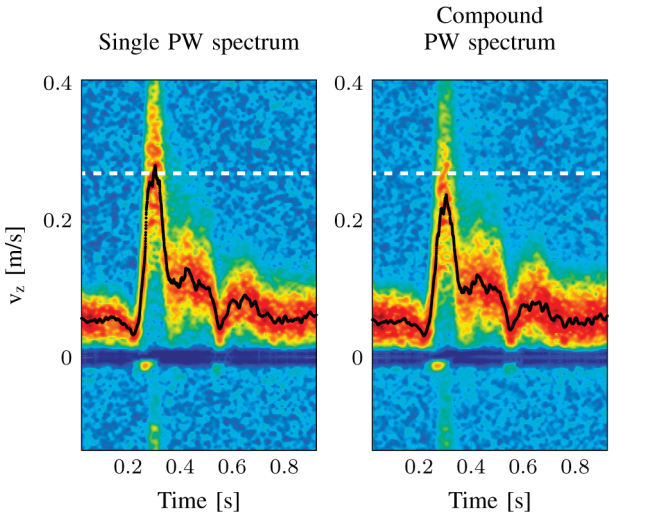

Fig. 9. PW Doppler spectra and mean velocity estimates (black line) from the common carotid artery of a healthy volunteer. Whereas in diastole some increase in signal power is found in the case of coherent compounding, there is a loss of signal power in systole, as well as a negative bias in the mean velocity. The PW spectra are shown with similar noise floor and 50 dB dynamic range. The white dashed line indicates the Nyquist velocity.

Although the results are based on plane wave coherent compounding, the conclusions are also relevant in other coherent compounding imaging scenarios in which high velocities are present, for instance, in cardiac applications using coherent compounding of diverging waves. Blood velocities larger than the Nyquist limit were also included for several reasons. In power Doppler imaging, the PRF is typically low to give high sensitivity to small vessels with slow blood flow. For CCD imaging however, lowering the PRF would result in large in-frame scatterer movement and therefore loss of SNR. In color flow imaging, peak velocities of 1.1 v_{Nyq} are not uncommon, because the PRF is set in a compromise between capturing low-velocity flow (ensure vessel filling and avoid dropouts) and high-velocity flow. In PW Doppler imaging, blood velocities are often high, especially in pathological cases, and the PRF is set as high as possible to capture the peak velocities. As in Fig. 9, it is also common to shift the baseline and include velocities up to 2 v_{Nyq} in the velocity spectrum. In situations with high blood flow velocities, the number of applicable angles for coherent compounding will be limited. However, because the properties of the compound filter changes little with N, blood velocities close to the Nyquist limit or with large beam-to-flow angles will yield negatively biased velocity estimates even when using only a small number of compound angles. In practical terms, the results suggest that whenever quantitative velocity measures are of interest from CCD imaging, means of avoiding the negative bias should be considered. These means include weighting of the echoes from different transmit angles, 2-D motion correction, or decreasing the beam-to-

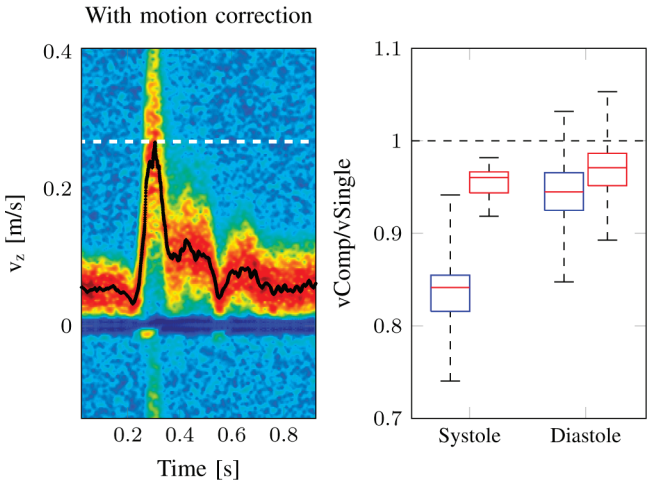

Fig. 10. (left): By correcting the coherent compounding at every timestep utilizing vector velocity estimates, spectral power at the highest velocities is regained, and the mean velocity estimates (black line) are closer to that of the single plane wave case. (right): Bias in mean velocity estimates before (blue boxes) and after (red boxes) motion correction in systole and diastole. Boxes show median values and the 25th and 75th percentiles of mean velocity estimates, whereas the whiskers account for the remaining values.

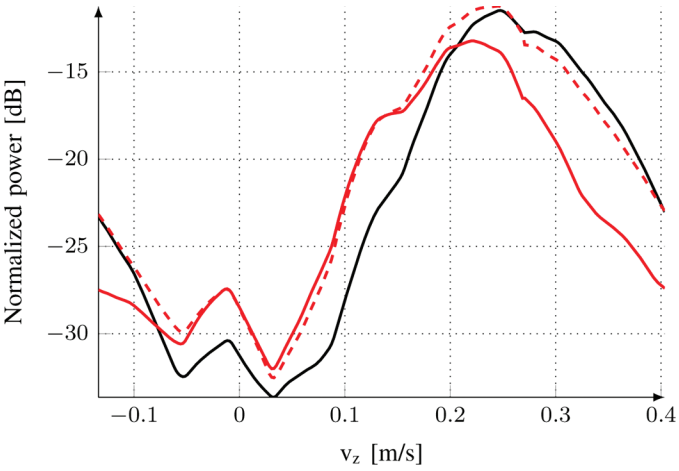

Fig. 11. Averaged power spectral estimates from 40 ms around peak systole. The black curve represents single plane wave imaging, whereas the red curves represent the power spectral estimates from CCD before (solid line) and after (dashed line) 2-D motion correction, respectively. The normalization is equal to that used for the full PW Doppler spectra in Figs. 9 and 10. It is observed that coherent compounding gives rise to spectral broadening due to the presence of larger beam-to-flow angles. These low frequencies will still be present after motion correction is performed.

flow angle. Although the effects of changing the receive focal number and apodization were not investigated here, a trade-off between image resolution and motion artifacts is expected: A smaller or more heavily apodized receive aperture will decrease image resolution, but will cause a longer transit time and might therefore reduce velocity bias and the loss in SNR.

The plug flow simulations showed good correspondence with the predicted values using the CCD signal model. This suggests that the low-pass filter interpretation is an adequate approximation of the effect of coherent compounding in Doppler, even though it does not include the effect of a varying beam-to-flow angle for the individual Doppler spectra. However, because some transmit angles will result in a reduced transit time compared with imaging in the reference direction, coherent compounding may cause increased spectral broadening. A significant amount of spectral broadening due to varying beam-to-flow angles can be expected to result in some residual bias being present after motion correction; this can, for instance, be observed in the *in vivo* velocity spectra shown in Fig. 11.

A 2-D motion compensation scheme based on multi-angle vector Doppler estimation was proposed, and further shown to substantially reduce the velocity bias and increase the Doppler SNR. Motion correction could therefore benefit both important quantitative measurements in larger vessels such as peak systolic velocity, but also detection of blood flow in small vessels for which high sensitivity is needed. Simulations demonstrated that 1-D motion correction was less effective in reducing the bias magnitude than 2-D correction. This was especially true for large beam-to-flow angles, which in the investigated imaging scenarios correspond to shorter transit times. In the cases with high-velocity and large BTF angles, signals from scatterers entering or leaving the beam during a frame are severely degraded. The increased benefit of using 2-D compared with 1-D correction could therefore be due to the slight increase in transit time obtained by reconstructing the CCD signal (amplitude and phase) correctly within every compound frame. A nonrectangular weighting of the echo amplitudes from different transmit angles was similarly shown to reduce the bias, although not to the extent of 2-D motion correction.

Plug flow was used in simulations to avoid influences of spatial gradients when averaging and in the flow phantom experiments, laminar, parabolic flow was ensured. The flow is also relatively simple in the common carotid artery which was used for the *in vivo* example. Further work will therefore focus on improving the robustness of multi-angle vector Doppler estimation and investigating the feasibility of using motion correction for more complex blood flow. In general, the accuracy of the vector Doppler estimates and therefore the motion correction will depend on the quality of the individual color flow images. However, as long as the signs of v_x and v_z are correct, motion compensation should benefit both PW Doppler spectra, mean velocity estimates and SNR. Aliasing was handled in this work by a simple unwrapping scheme. However, more robust means to correct for aliasing, as demonstrated for multi-angle vector Doppler imaging in [13] and [14], should be included, because aliasing, in addition to signal dropouts due to clutter filtering, is the main factor degrading vector Doppler estimates. Increasing the number of transmit and/or receive angles will also increase the redundancy of the estimation problem and therefore also the accuracy.

It was found that 1-D and 2-D motion correction resulted in similar gain in Doppler SNR, a result that could be expected given the higher spatial frequency content in the depth direction. The impact of radial motion on SNR and contrast when utilizing coherent compounding for B-mode imaging has been investigated previously [10]. It was shown that large radial velocities cause significant loss in these image parameters when the coherent compound image is fully sampled. However, downsampling the sequence by reducing the number of transmit angles while keeping the angle span reduced these effects, yielding an SNR loss compared with stationary tissue of approximately 2 dB at velocities close to the Nyquist limit. Our results support these findings, which means that the presence of a negative bias might be the more important artifact for Doppler imaging. Still, in cases in which the SNR is low, as is often the case with blood flow imaging, a loss of 2 dB could be significant. In cases in which the blood velocity is larger than the Nyquist limit, the loss in SNR may be even higher (4 dB at $1.1 \cdot v_{\mathrm{Nyq}}$) and might result in significantly reduced sensitivity in power Doppler imaging.

V. Conclusion

Coherent compounding in Doppler acts as a low-pass filter, and will result in negatively biased Doppler spectra

and mean velocity estimates. The magnitude of the bias increases with increasing velocity and/or beam-to-flow angle, reducing the quantitatively useful velocity span in CCD imaging. Increasing the velocity or beam-to-flow angle results in a decreased Doppler SNR and therefore loss in power Doppler imaging sensitivity. However, by using 2-D motion correction, it is possible to reduce the bias substantially and obtain an SNR which is less dependent on blood flow velocity and direction.

References

[1] L. Lovstakken and H. Torp, "Extended velocity range in color flow imaging using parallel receive beamforming," in *IEEE Int. Ultrasonics Symp.*, 2010, pp. 1198–1201.

[2] J. Bercoff, G. Montaldo, T. Loupas, D. Savery, F. Mézière, M. Fink, and M. Tanter, "Ultrafast compound Doppler imaging: Providing full blood flow characterization," *IEEE Trans. Ultrason. Ferroelectr. Freq. Control*, vol. 58, no. 1, pp. 134–147, 2011.

[3] I. K. Ekroll, A. Swillens, P. Segers, T. Dahl, H. Torp, and L. Lovstakken, "Simultaneous quantification of flow and tissue velocities based on multi-angle plane wave imaging," *IEEE Trans. Ultrason. Ferroelectr. Freq. Control*, vol. 60, no. 4, pp. 727–738, 2013.

[4] G. Montaldo, M. Tanter, J. Bercoff, N. Benech, and M. Fink, "Coherent plane-wave compounding for very high frame rate ultrasonography and transient elastography," *IEEE Trans. Ultrason. Ferroelectr. Freq. Control*, vol. 56, no. 3, pp. 489–506, 2009.

[5] E. Mace, G. Montaldo, B. F. Osmanski, I. Cohen, M. Fink, and M. Tanter, "Functional ultrasound imaging of the brain: Theory and basic principles," *IEEE Trans. Ultrason. Ferroelectr. Freq. Control*, vol. 60, no. 3, pp. 492–506, 2013.

[6] S. I. Nikolov and J. A. Jensen, "In-vivo synthetic aperture flow imaging in medical ultrasound," *IEEE Trans. Ultrason. Ferroelectr. Freq. Control*, vol. 50, no. 7, pp. 848–856, 2003.

[7] J. A. Jensen and S. I. Nikolov, "Directional synthetic aperture flow imaging," *IEEE Trans. Ultrason. Ferroelectr. Freq. Control*, vol. 51, no. 9, pp. 1107–1118, 2004.

[8] E. Macé, G. Montaldo, I. Cohen, M. Baulac, M. Fink, and M. Tanter, "Functional ultrasound imaging of the brain," *Nat. Methods*, vol. 8, no. 8, pp. 662–664, 2011.

[9] G. E. Trahey and L. F. Nock, "Synthetic receive aperture imaging with phase correction for motion and for tissue inhomogeneities. II. Effects of and correction for motion," *IEEE Trans. Ultrason. Ferroelectr. Freq. Control*, vol. 39, no. 4, pp. 496–501, 1992.

[10] B. Denarie, T. A. Tangen, I. K. Ekroll, N. Rolim, H. Torp, T. Bjastad, and L. Lovstakken, "Coherent plane wave compounding for very high frame rate ultrasonography of rapidly moving targets," *IEEE Trans. Med. Imaging*, vol. 32, no. 7, pp. 1265–1276, 2013.

[11] N. Oddershede and J. Jensen, "Effects influencing focusing in synthetic aperture vector flow imaging," *IEEE Trans. Ultrason. Ferroelectr. Freq. Control*, vol. 54, no. 9, pp. 1811–1825, 2007.

[12] K. Gammelmark and J. A. Jensen, "2-D tissue motion compensation of synthetic transmit aperture images," *IEEE Trans. Ultrason. Ferroelectr. Freq. Control*, vol. 61, no. 4, pp. 594–610, 2014.

[13] J. Flynn, R. Daigle, L. Pflugrath, K. Linkhart, and P. Kaczkowski, "Estimation and display for vector Doppler imaging using planewave transmissions," in *IEEE Int. Ultrasonics Symp.*, 2011, pp. 413–418.

[14] B. Y. Yiu, S. S. Lai, and A. C. Yu, "Vector projectile imaging: Time-resolved dynamic visualization of complex flow patterns," Ultrasound Med. Biol., vol. 40, no. 9, pp. 2295–2309, 2014.

[15] J. A. Jensen, "Field: A program for simulating ultrasound systems," *Med. Biol. Eng. Comput.*, vol. 34, suppl. 1, pt. 1, pp. 351–353, 1996.

[16] C. Kasai, K. Namekawa, A. Koyano, and R. Omoto, "Real-time two-dimensional blood flow imaging using an autocorrelation technique," *IEEE Trans. Sonics Ultrason.*, vol. 32, no. 3, pp. 458–464, 1985.

[17] D. Rickey, P. Picot, D. Christopher, and A. Fenster, "A wall-less vessel phantom for Doppler ultrasound studies," *Ultrasound Med. Biol.*, vol. 21, no. 9, pp. 1163–1176, 1995.

[18] K. Ramnarine, D. Nassiri, P. Hoskins, and J. Lubbers, "Validation of a new blood-mimicking fluid for use in Doppler flow test objects," *Ultrasound Med. Biol.*, vol. 24, no. 3, pp. 451–459, Mar. 1998.

Ingvild Kinn Ekroll was born in Ålesund, Norway, in 1984. She earned a master's degree in biophysics and medical technology in 2009, and a Ph.D. degree in medical technology in 2013, both from the Norwegian University of Science and Technology (NTNU), Trondheim, Norway. She is currently working as a researcher with the Department of Circulation and Medical imaging at NTNU, focusing on different aspects of Doppler ultrasound signal processing and ultrasound imaging of blood flow in general.

Marco M. Voormolen was born in Utrecht, The Netherlands, in 1972. He earned his M.Sc. degree in measurement and control engineering and biomedical engineering in 1998 from the University of Twente, The Netherlands. Starting in 1999, he worked as consultant on safety and control systems for the railway industry. In 2001, he took a position as a Scientific Researcher at the Department of Biomedical Engineering at the Erasmus University Medical Center in Rotterdam, where, in addition, he successfully pursued his Ph.D. degree. His Ph.D. dissertation, entitled "3D Harmonic Echocardiography," involved nonlinear acoustic theory, 3-D echocardiographic imaging techniques, and image processing. In 2008, Marco moved to Trondheim to take a postdoctoral position at the Norwegian University of Science and Technology (NTNU), where he focused on transducer technology for high-frequency ultrasonic applications. From 2011 to 2013, he was employed by Aurotech Ultrasound, where he was involved in regulatory affairs and management of client portfolios. In 2013, Marco joined InPhase Solutions as project manager and co-owner; he also holds a part-time researcher position at the NTNU.

Oyvind K.-V. Standal was born in Lørenskog, Norway, in 1976. He received his M.Sc. degree in applied mathematics from the Norwegian University of Science and Technology (NTNU) in 2002. From 2003 to 2011, he was employed as a researcher and laboratory engineer at the Department of Circulation and Medical Imaging at NTNU, where he worked on instrumentation and signal analysis. Øyvind has been a Senior Consultant at InPhase Solutions AS since 2011.

Jochen Rau was born in Germany in 1980. He studied at RWTH Aachen University, Aachen, Germany, where he earned his Dipl.-Ing. degree in electrical engineering and information technology in 2006. He received the Ph.D. degree in medical technology from the Norwegian University of Science and Technology (NTNU), Trondheim Norway, in 2013. He is currently working as researcher with the Department of Circulation and Medical Imaging at NTNU and as consultant at InPhase Solutions, Trondheim, Norway. His main ultrasound research interests include nonlinear imaging, reverberations/clutter, array design, and instrumentation.

Lasse Løvstakken was trained in engineering cybernetics (M.Sc.) and medical ultrasound imaging technology (Ph.D.) at the Norwegian University of Science and Technology (NTNU), and is currently a professor in the Department of Circulation and Medical Imaging at NTNU. His main research interests include signal and image processing applied in medical ultrasound imaging for improved image formation, and for the detection and estimation of moving tissue and blood flow. His main clinical focus has been cardiovascular imaging with emphasis on methods for improved estimation of blood velocities in the heart and vessels.